Influence of hygrothermal environment on thermal and mechanical properties of carbon fiber/fiberglass reinforced matrix composite materials

Y.I. Tsai[1], E.J. Bosze[1], E. Barjasteh[1], S.R. Nutt[1*]

1. Department of Chemical Engineering and Materials Science, University of Southern California, 3561 Watt way, VHE-602 Los Angeles, CA 90089, USA

Abstract: The absorption and diffusion of water in a carbon fiber/glass fiber hybrid composite was investigated. Water-sorption experiments, mechanical property tests and dynamic mechanical analysis (DMA) were performed after immersion in water at different temperatures for up to 32 weeks. The moisture uptake mechanism exhibited by the hybrid fiber system was determined to be more complex than the single fiber type. Weight-change profiles for the composites fitted the theoretical Fickian diffusion curve during the initial immersion time, but diverged substantially as time progressed. The shear properties and the glass transition temperature (Tg) were sensitive to the effects of hygrothermal environment, and values for both decreased with increasing water uptake. Microscopic inspection of water-soaked samples showed no cracking when the absorption was less than saturation. The thermal and mechanical properties were mostly retained (after drying), provided the moisture absorption did not exceed the saturation point.

Key words: A. Carbon fibers; A. Glass fibers; B. Hygrothermal effect; B. Interface; C. Crack

1. Introduction

In recent years, the advent of commercial-grade carbon fiber and low-cost manufacturing processes has led to new applications for composite materials in industrial sectors outside of aerospace and

Please cite this article as: Y-I Tsai, E.J. Bosze, E. Barjasteh, and S.R. Nutt; **Influence of hygrothermal environment on thermal and mechanical properties of carbon fiber/fiberglass reinforced matrix composite materials**, Compos. Sci. & Technol.69 [3-4] (2009) 432-437, DOI:http://dx.doi.org/10.1016/j.compscitech.2008.11.012

recreational products. One example of an emerging non-aerospace application is the composite reinforcement of high-voltage overhead conductors, which may eventually replace conventional steel-reinforced conductors and have a major impact in the power industry [1] and [2].

The effects of environmental exposure of fiber-reinforced polymer composites (FRPC) and the long-term retention of properties are significant concerns for such applications, where the service life can span several decades and little or no maintenance is expected. To design for such service life requires the ability to forecast changes in material properties as a function of environmental exposure, including bulk properties and the integrity of fiber–matrix interfaces. For overhead conductors, environmental attack results primarily from exposure to temperature, moisture, radiation, aggressive chemicals and combinations of these factors with mechanical loads. These factors can (and generally do) affect the mechanical and physical properties of composites in adverse ways, as described in multiple studies [3], [4], [5], [6], [7] and [8].

Moisture in any form is unfriendly for polymer composites, and often causes swelling and degradation. Matrix and/or interface degradation resulting from moisture absorption is a concern in most composite applications subject to normal atmospheric moisture, which can range from precipitation to mild humidity. Complete immersion in water constitutes the most severe environment, while humid air generally results in lower maximum moisture content [9], [10] and [11].

Long-term exposure at high temperatures is generally a secondary concern for FRPCs, provided the temperature does not approach the glass transition temperature of the matrix. Liao et al. reported that moisture absorption induced larger strains than high temperature exposure for unidirectional polymer composites, primarily because the coefficient of moisture expansion was greater than the coefficient of thermal expansion [12]. However, higher temperatures accelerate diffusion rates of

moisture and generally accelerate aging. Various aspects of moisture-induced behavior and the dependence on such factors have been studied, and both Fickian and non-Fickian diffusion behavior have been reported [5], [6], [7], [8], [11], [13], [14], [15], [16] and [17].

In this paper, we report the effects of moisture absorption on a unidirectional hybrid composite material developed to support overhead conductor lines [1], [2] and [18]. The hygrothermal effect on the thermal and short beam shear properties was investigated and analyzed. Moisture content, short beam shear strength and glass transition temperature are compared and correlated.

2. Experimental Procedure

2.1Materials

The hybrid fiber composite used in this study was a unidirectional carbon fiber (CF)/glass fiber (GF) reinforced composite rod, 9.53 mm in diameter, as shown in Fig. 1. The composite rod, which was designed for supporting overhead conductor lines, was manufactured by pultrusion using a propriety epoxy formulation and an anhydride curing agent. The outer shell of the composite rod was reinforced with fiberglass while the internal core was reinforced with carbon fiber. The diameter of CF core was ~7 mm, and the total fiber volume fraction was ~67%. In addition, control samples comprised of all-CF and all-GF composite 6.3 mm rods were produced as the control group to compare diffusion coefficients and behavior.

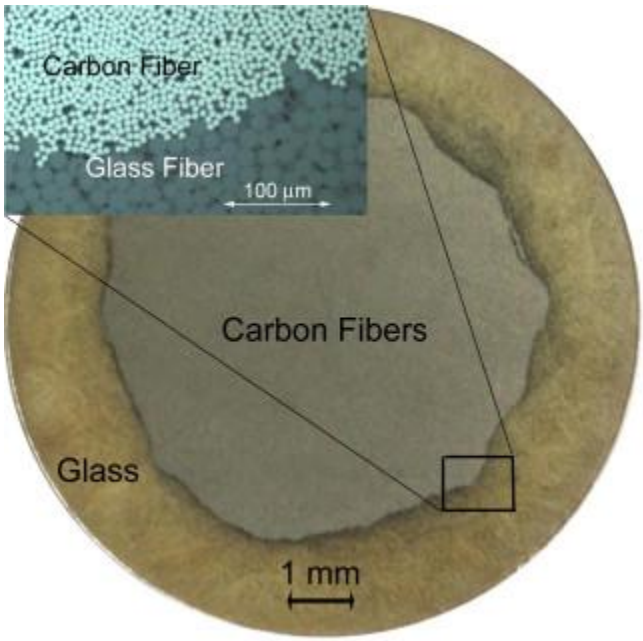

Figure 1: *Cross-section of the pultruded composite core, showing the carbon composite in the center and the glass composite shell around it.*

2.2 Conditioning

Samples were cut to a length of 66.5 mm using a diamond saw, and silicone sealant was applied to the specimen ends to prevent moisture penetration on the cut ends. Prior to water immersion, all specimens were dried in a 100 °C oven for 2 days to remove retained moisture. To assess dryness, a few samples were dried for 8 days at 100 °C, producing a slight additional weight loss that was 3% greater than the weight loss after the standard drying time of 2 days. All samples were then weighed using an analytical balance (ACCULAB LA-60) with 0.01 mg accuracy. The specimens were then placed in large Pyrex dished containing de-ionized water at 40 °, 60 ° and 90 °C, separated by wire mesh to avoid specimen contact. Samples were removed from the baths at predetermined times up to 32 weeks. All samples were subsequently weighed to determine weight change. The weight gain was calculated according to:

$$\frac{W_w - W_o}{W_o} \times 100\% \quad (1)$$

where W_w is the wet weight and Wo is the dry weight.

After weighing, the specimens were divided into two groups of three samples each. The first group was not dried, and the short beam shear (SBS) strength and Tg was determined in the "wet" state. The second group of samples was dried in a 100 °C oven for 2 days to stabilize the weight, and then the same measurements were performed. Drying the second set of samples was performed to determine if any decrease in property values was reversible by removing the absorbed moisture.

2.3 Short beam shear, thermal properties and visual determination

The influence of the hygrothermal environment on the mechanical and thermal properties was studied. SBS strength testing was measured in accordance with ASTM D4475-02 in a commercial instrument (INSTRON 5567), using a span length 6 times the diameter and a crosshead displacement rate of 1.3 mm/min. Dynamic mechanical analysis (DMA) was performed to determine the shift of Tg. A dual cantilever beam clamp was employed using a commercial instrument (TA Instruments DMA2980). Rectangular samples (60 × 9.5 × 1.6 mm) sectioned from the CF core of the rod were measured and the Tg was determined from the peak in the loss modulus curve. Transverse sections were cut and polished using conventional polishing techniques and then examined microscopically to detect evidence of cracking with different exposure times. In addition, dye penetrate was used to detect cracks in the composite samples.

3. Results

3.1 Moisture absorption

The moisture absorption behavior is shown in Fig. 2, where the percent weight gain is plotted as a function of the square root of the immersion time ($s^{1/2}$) for different temperatures. Each point represents the average of measurements on six specimens, and the error bar is the standard deviation value. The weight gain values for the 40, 60 and 90 °C baths after 5300 h (32 weeks) were 0.53 ± 0.03%, 0.90 ± 0.04% and 11.74 ± 1.22% respectively. The solid lines are the theoretical Fickian diffusion curves obtained by fitting the moisture absorption, M_t, equation [19]:

$$M_t = \left[1 - \sum_{n=1}^{\infty} \frac{4}{a^2 \alpha_n^2} \exp(-D\alpha_n^2 t)\right] M_\infty \tag{2}$$

where M_∞ is the saturation level of water absorption, D is the diffusion coefficient, a is the radius and α_n is the nth root of the zero order Bessel function. The Bessel function appears in this equation because of the cylindrical geometry of the samples. The saturation level M_∞ is assumed to be a constant for the case of complete immersion in water [9] without any cracking mechanism. By fitting the initial slope to Eq. (2) and choosing 1% as the assumed saturation point (the value of 1% was chosen based on a fit to the theoretical diffusion curve), D can be determined, and the values for each water temperature are shown in Table 1. Below the saturation level, moisture absorption was responsible for the observed weight gain. Above the saturation point, the development of cracks resulted in large weight gain increases due to trapping of infiltrated water. This study primarily concerned the moisture absorption mechanism. Fig. 3 shows a plot of diffusion coefficient (ln D) versus inverse temperature, yielding the expected linear dependence [7].

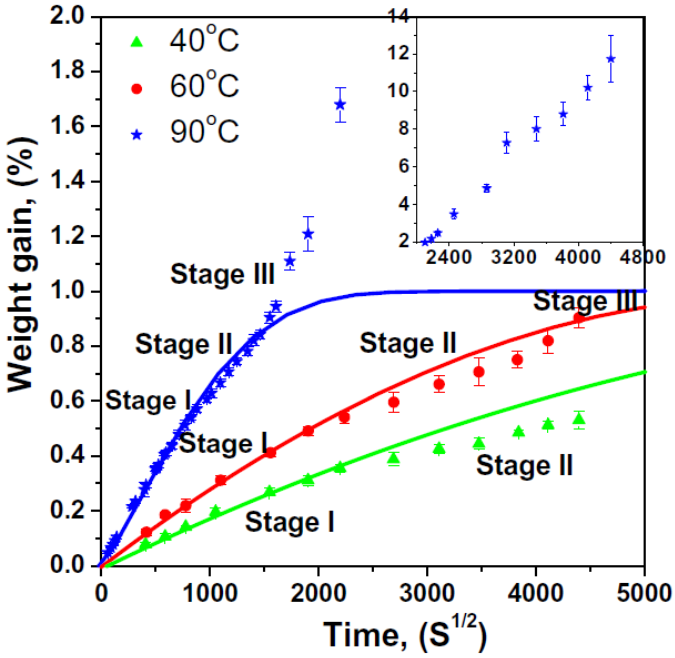

Figure 2: *Weight gain versus the square root of time ($s^{1/2}$) for composites immersed in 40 °C, 60 °C and 90 °C water.*

Table 1: *Initial diffusivity coefficients for each of the water immersion experiments.*

Temperature (°C)	**40**	**60**	**90**
D ($m^2 s^{-1}$)	1.42×10^{-13}	3.84×10^{-13}	2.7×10^{-12}

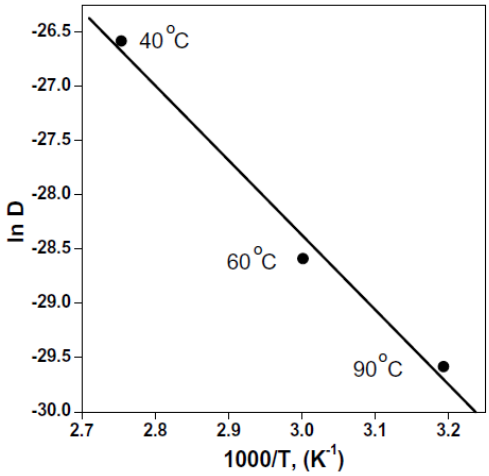

Figure 3: *Diffusivity coefficient variation with temperature.*

Plots of moisture content distribution as a function of radial position within the composite are shown in Fig. 4a–c for the 40, 60 and 90 °C exposures. The numbers on the curves represent different exposure times, given in $s^{1/2}$, which were used to calculate the moisture concentration levels inside the rods. The curves at specific times were determined [18]

$$C(r,t) = 1 - \frac{2}{a}\sum_{n=1}^{\infty}\frac{\exp(-D\alpha_n^2 t)J_0(r\alpha_n)}{\alpha_n J_1(a\alpha_n)} \tag{3}$$

where r is the radial position of the specimen, t is the time, J_0 is the Bessel function of zero order, J_1 is the Bessel function of first order, and D is the diffusion coefficient at each temperature, listed in Table 1. The GF/CF interface is located at ~3.5 mm in these figures and is an important region for the moisture absorption mechanism.

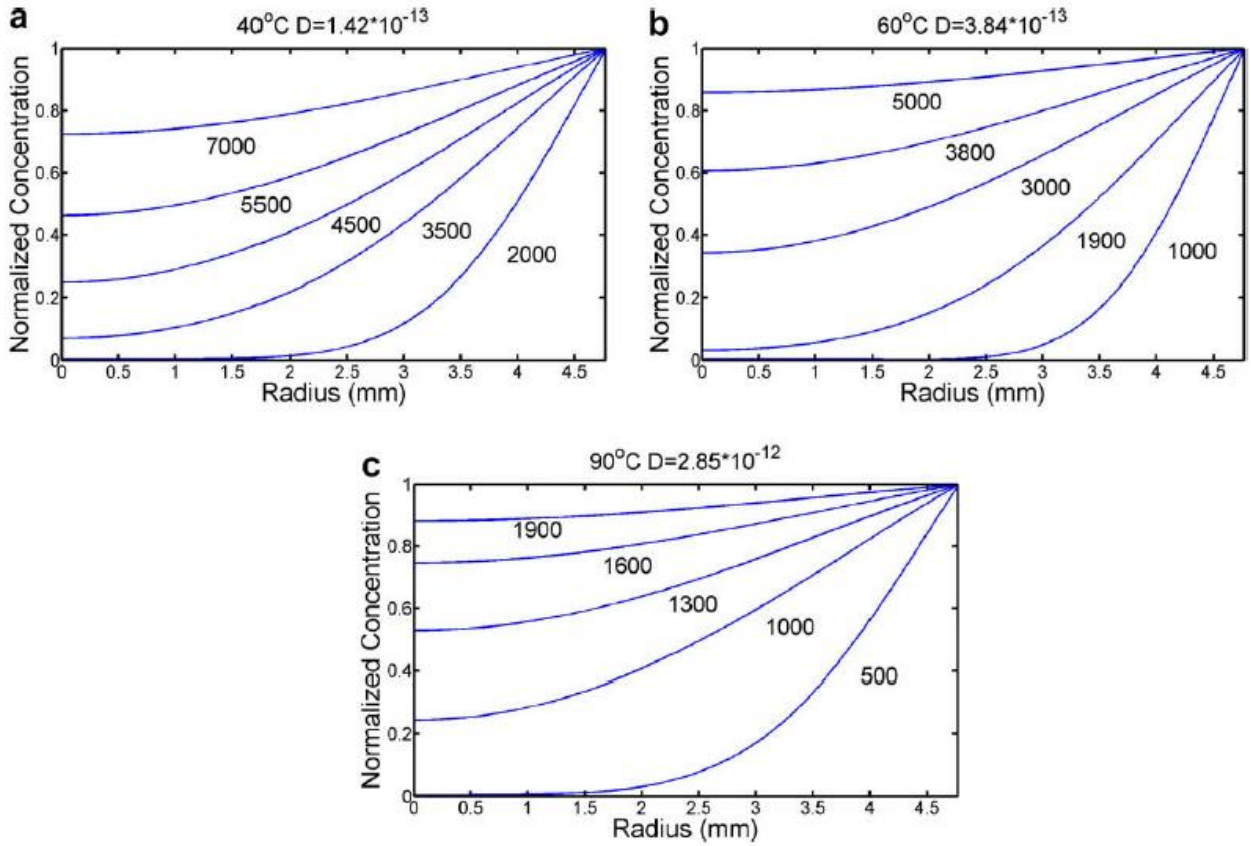

Figure 4: *Moisture concentration distribution-radial position profiles for (a) 40 °C, (b) 60 °C and (c) 90 °C water.*

In this study, the 40 and 60 °C samples did not reach saturation in 32 weeks, and 90 °C samples apparently exceeded the assumed saturation level of 1%. Fig. 2 indicated that the weight gain data for the 40, 60 and 90 °C samples are coincident with the theoretical Fickian curves for the first 1344 h (~2200 $s^{1/2}$), 1000 h (~1900 $s^{1/2}$) and 625 h (~1500 $s^{1/2}$), respectively. The 40 and 60 °C samples showed non-Fickian behavior before reaching the saturation point. To determine if the deviation from the predicted behavior was attributable to phenomena peculiar to the CF/GF interface, all-CF and all-GF composite rods were exposed to 60 °C water. These rods were 6.3 mm in diameter, smaller than the 9.53 mm of the hybrid GF/CF rods used earlier, and the fiber volume fractions were greater (75% versus 70%). Because of the slightly higher fiber loading, the rods saturated to a slightly lower moisture level (0.85% versus 1%), as shown in Fig. 5. More significantly, the absorption curves show no evidence of a change in the diffusion rate before saturation. The distinctly different behavior of the hybrid composites is attributed primarily to the presence of the radial GF/CF interface.

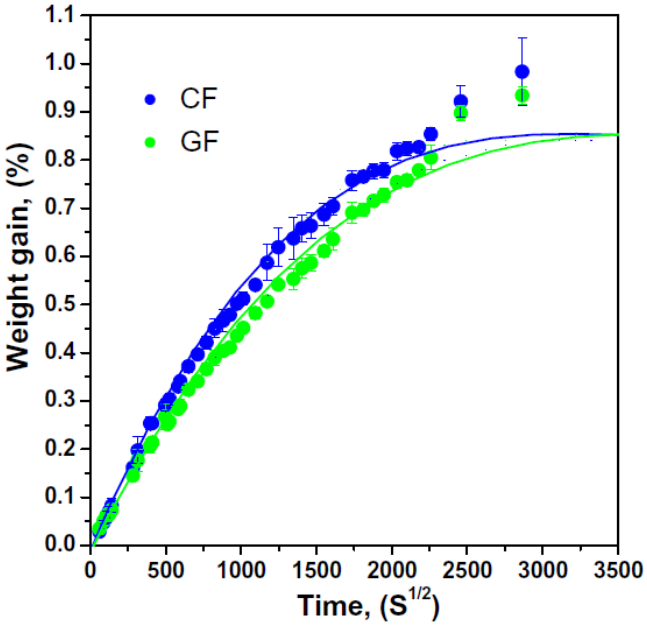

Figure 5: *The percent weight gain at 60 °C as a function of time for all-GF and all-CF 6.3 mm diameter rods.*

3.2Changes in the physical and mechanical properties and physical characteristics

As the amount of water absorbed by the composite increased over time, reductions in the $T_g$and SBS strength were measured. The change in the T_g as a function of the water temperature and time is presented in Fig. 6a, and shows that the hygrothermal environment strongly affects the rate at which T_g decreases. Fig. 6b shows the correlation between $T_g$and percent moisture absorption. For equivalent levels of moisture absorption, exposure at higher temperatures yields higher values of T_g (or smaller decreases). For example, for a weight increase of 0.5%, the T_g values were 165 °C, 175 °C and 190 °C for exposures at 40 °C, 60 °C and 90 °C, respectively. Thus, for a specific moisture level, the lower exposure temperatures resulted in lower values of T_g. The reason for this curious behavior stems from the different distributions of moisture in the rods, as shown in Fig. 4,

and the fact that the $T_g$measurements were performed by sectioning beams from the rod cores, where the local moisture levels differed from the global moisture concentration. Higher exposure temperatures produced steeper concentration profiles, resulting in smaller decrements inT_g. The inset in Fig. 6b shows how the T_g changed over the entire exposure time. Table 2shows the original T_g values and the reduced values after moisture exposure (for the 90 °C exposure, the reported T_g value corresponds to 1% moisture saturation). At 40 and 60 °C, the composites had not reached saturation even after 32 weeks.

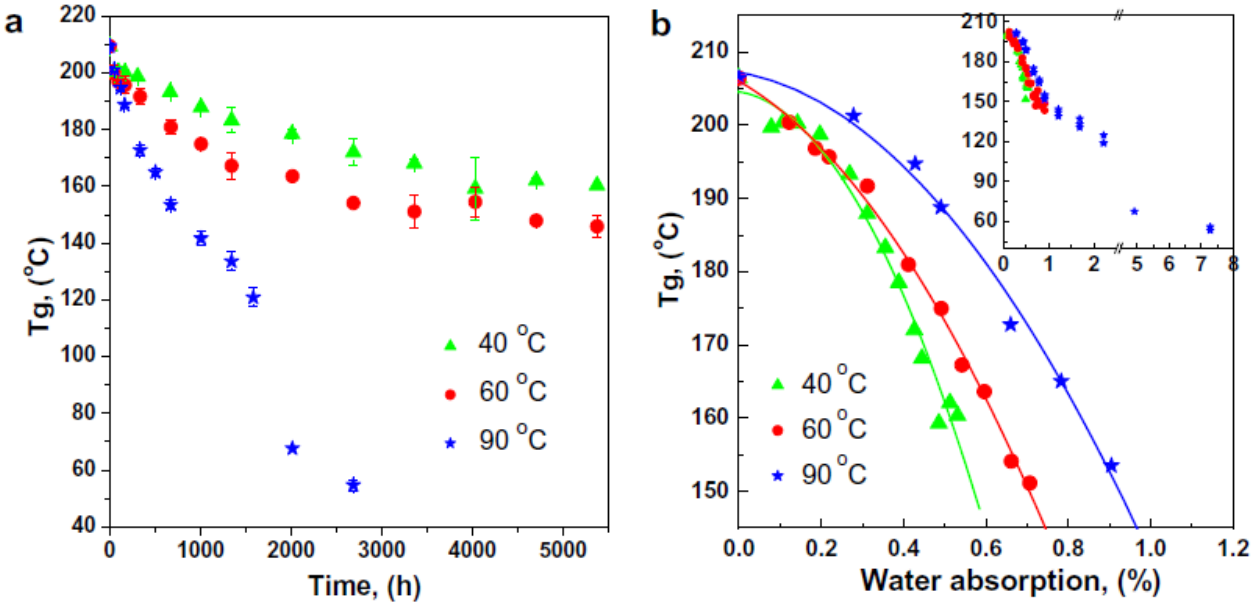

Figure 6: *(a) The change in the T_g as a function of the water temperature and time. (b) The change in T_g as a function of percent water absorption in the initial period with water temperature at less than 1% water absorption. The inset shows the complete data.*

Table 2: *Reduction (Red.)/retention (Ret.) of the SBS and T_g properties after immersion in water at 40 °C, 60 °C (for 32 weeks) and 90 °C (for 4 weeks).*

	Shear strength (MPa)	**Red./Ret. (%)**	**T_g (°C)**	**Red./Ret. (%)**
Start	48	0	209	0
40 °C (32 Weeks)	41.8/47.2	87/98	160.3/189.5	77/91
60 °C (32 Weeks)	38.2/40.7	80/85	146/160.2	70/77
90 °C (4 Weeks)	37/41.8	77/87	153.5/168.4	73/81

The dependence of the SBS strength on the hygrothermal environment is shown in Fig. 7.Fig. 7a shows the dependence of the SBS strength on time and exposure temperature, while Fig. 7b shows the SBS dependence on water absorption level. Table 2 shows the original SBS values and the reduced values after exposure. The reductions in T_g and SBS strength with water sorption show similar trends that are apparent by comparing Fig. 6 and Fig. 7.

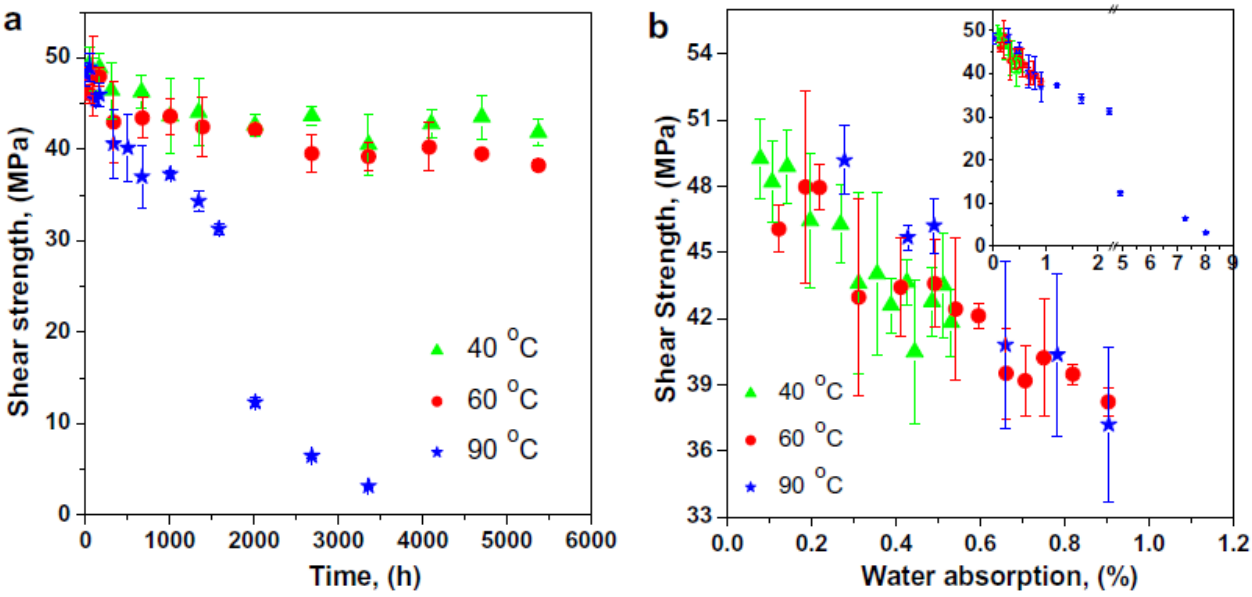

Figure 7: *(a) The change in the short beam shear strength as a function of time and water temperature. (b) The strength as a function of the water absorption amount in the initial period with water temperature at less than 1% water absorption. The inset shows the complete data.*

Sample discoloration was observed after extended exposures. The composite rods changed from brown to a tan/white color, which is attributed to changes in the matrix chemistry, as reported elsewhere [6]. The surface condition of the samples also showed different degrees of change. The surface of 40 °C samples remained smooth, much like the unaged composite surface. However, samples that were exposed at 60 and 90 °C exhibited rougher surfaces because of partial debonding of glass fibers at the surface.

3.3Recovery of physical and mechanical properties

The reversibility of mechanical and physical properties after moisture exposure was assessed in this study. The recovery and percent retention of thermal and mechanical properties are shown in Table 2. Samples exposed to 40 and 60 °C for 32 weeks showed 85–98% recovery in SBS strength and 77–91% recovery of Tg after drying. Samples exposed at 90 °C for 4 weeks that were near the saturation point also showed the comparable retention. Thus for moderate time–temperature exposures, the composites retained Tg and SBS strength to a large degree before reaching the critical saturation level.

In summary, removal of moisture resulted in near full recovery of both Tg and SBS strength, while the moisture level was below saturation. However, once the assumed saturation of 1% was exceeded, these properties did not fully recover and the exposure caused permanent damage to the matrix. In particular, when moisture levels exceeded 2%, the damage was manifest in cracks. The unusually high moisture content in the 90 °C samples is tentatively attributed to moisture entrapped in cracks, although this assertion awaits further investigation.

4. Discussion

The hybrid composite features a thick outer GF shell and a CF core, each comprising ~50% of the cross section. The GF shell is intended to prevent galvanic coupling between the CF core and the overlaid aluminum wires of the overhead conductor [1], [20] and [21]. This core–shell structure of the hybrid composite is largely responsible for the complex pre-saturation behavior observed in Fig. 2, which was noticeably different from the diffusion behavior exhibited by the all-GF and all-CF control samples, shown in Fig. 5. In the hybrid composite system, moisture first penetrated the outer GF shell and diffused to the GF/CF interface. While the moisture concentration of the GF shell approached the critical level, the GF/CF interface dominated the diffusion behavior by acting as a moisture barrier, as explained below.

Samples immersed at 40 and 60 °C did not reach saturation in the 32-week exposure period, and two stages of moisture absorption were observed. In contrast, the 90 °C exposures reached the theoretical saturation level within 672 h, and a third stage was observed, associated with irreversible cracking damage. The first two stages of moisture uptake followed the theoretical moisture diffusion behavior without the cracking issue. Because the anticipated service temperatures for the overhead conductors are 50–180 °C, the moisture concentration should never reach the saturation level. Thus, the first two stages that occurred below the saturation level are of primary interest in the present study.

Stage I. The weight gain data are accurately described by fitting a theoretical Fickian curve in this stage. The diffusion kinetics during Stage I are primarily determined by the GF shell. The stage ended when the moisture content in the GF shell reached a critical level. At this point, the diffusion rate apparently changed. For exposures at 40 and 60 °C, the slope of weight gain changed at 2200 and 1900 $s^{1/2}$, respectively, as shown in Fig. 2, signaling the end of Stage I. Fig. 4 shows that the

moisture content reached 70–75% of saturation in the GF shell and was between 35% and 50% at the GF/CF interface in the end of stage I, depending on the temperature. In contrast, there was no clear indication between Stage I and II for 90 °C specimens.

Stage II. The GF/CF interface played an important role as moisture barrier in Stage II, altering the diffusion mechanism. In this period, the diffusion rate apparently decreased due to the inhomogeneity of the GF/CF interface. The 40° and 60 °C samples ended the experiment during Stage II, but the final data point of the 60 °C sample showed a sudden increase in diffusion rate, suggesting the possible onset of Stage III, although no additional data were recorded.

Stage III. In this period, the slope of the weight gain curve sharply increased and the value of weight gain quickly exceeded the theoretical 1% saturation point. The onset of Stage III for the 90 °C exposures occurred at a weight gain of ~0.8%. At this point, the water content at the GF/CF interface reaches 80–90% of saturation and the GF shell was completely saturated as shown in Fig. 4c. The slope of the weight gain curve in this period was attributed to the microcracking which developed after exceeding the theoretical 1% saturation level [5]. However, evidence of cracking in 90 °C samples appeared at >2.1% weight gain, when multiple macrocracks appeared along the CF/GF interface.

The change in diffusion rate between stages I and II observed in Fig. 2 was clearly associated with the GF/CF interface, and multiple explanations were considered to explain this phenomenon. First, the difference in CF and GF fiber diameters could cause an increase in path length, introducing a tortuosity factor which is inversely related to the diffusion rate [22] and [23]. This phenomenon was examined by simply calculating the increase in the path length around the fibers and comparing the new length to the length of a straight line connecting the same start and end points. However,

calculations revealed no significant difference (<5%) in the diffusion path length for the GF shell and the CF core.

Closer examination of the GF/CF interface revealed a slight inter-mingling of CF with the larger GF, resulting in closer packing, as shown in Fig. 8. The smaller CFs (~7 μm) inserted into the space between the larger GFs (~20 μm). Image analysis using the linear intercept method revealed that the fiber loadings of the core and shell regions were 67%. However, the local fiber loading at the GF–CF interface was ~75%. Consequently, the diffusion path was changed from the relatively wide inter-fiber spacing of GF shell to the narrow inter-fiber spacing at GF/CF interface region. The closer packing at the annular interface region retards the diffusion of moisture, and acts as an effective (albeit accidental) moisture barrier.

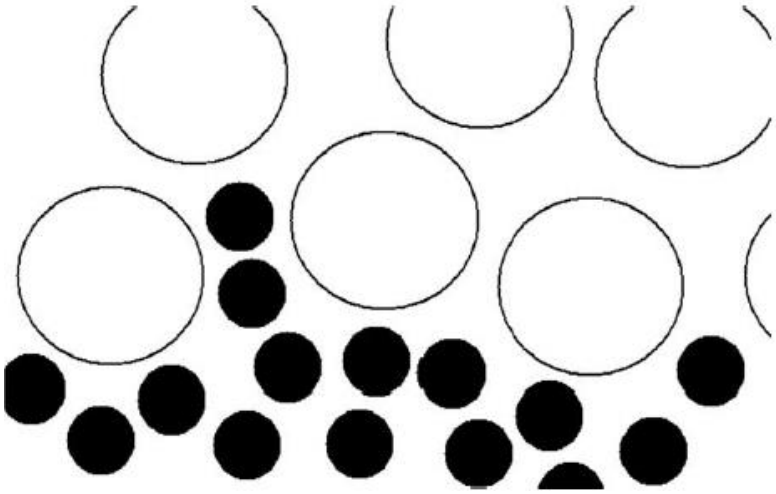

Figure 8: *Schematic of the carbon fiber/glass fiber interface region.*

As expected, temperature also affected the diffusion kinetics. Because the *D* of the 90 °C samples was nearly two and 1.5 times the rate of the 40 and 60 °C samples, respectively, the diffusion kinetics was not slowed by the GF/CF interface, unlike the samples exposed at lower temperatures. Polished cross sections of the 40 and 60 °C samples showed no evidence of micro- or macro-cracking after

32 weeks immersions, and attempts to detect microcracks using fluorescent dye penetrator were also negative. Polished cross sections of 90 °C samples near the saturation point (at the end of the stage I/II) showed no evidence of microcracking.

Degradation resulting from the hygrothermal environment is often caused by damage to the fiber/matrix interface, and generally results in a decrease in strength and modulus [15]. Moisture absorption also softens the matrix, degrading the stress transfer function and resulting in a substantial loss of T_g and SBS strength. In this study, removal of absorbed moisture led to significant recovery (77–98%) of original values for thermal and mechanical properties. However, full recovery was not achieved, showing that at least some permanent damage occurred.

5. Conclusions

Accelerated aging experiments were conducted to determine the moisture uptake behavior for the hybrid GF/CF composite rod developed for supporting overhead conductors. The hybrid composite exhibited more complex moisture absorption behavior than the single fiber-reinforced composite material. The complex behavior was attributed to a higher density packing of fibers located at the annular GF/CF interfaces region, which acted as a temporary moisture barrier. The existence of GF/CF interface is not uncommon in composites, particularly in composites intended for overhead conductors. In aerospace applications, it is common practice to insert a thin layer of fiberglass between metallic structures and attached CF composite parts to prevent galvanic corrosion. However, in the present study, the GF/CF interface is embedded deep beneath the outer surface, and each constituent comprises ~50% of the cross section. Thus, the water absorption behavior is quite different from typical aerospace parts, with the GF layer dominating the diffusion rate for a long

time before the CF region even begins to influence the diffusion behavior. Finally, as long as the water concentration in the sample was less than the saturation level, the SBS strength and T_g showed 77–98% retention in their respective properties after removing the absorbed moisture. Thus, sub-saturation levels of absorbed moisture caused only moderate damage to fiber–matrix interfaces.

Acknowledgements: The authors are grateful to Composite Technology Corporation for supporting this work.

References:

1. Alawar A, Bosze EJ, Nutt SR. *A composite core conductor for low sag at high temperatures*. IEEE Trans Power Delivery 2005;**20**(3):2193–9.
2. Bosze EJ, Alawar A, Bertschger O, Tsai YI, Nutt SR. *High-temperature strength and storage modulus in unidirectional hybrid composites*. Comp Sci Tech 2006;**66**:1963–9.
3. Selzer R, Friedrich K. *Mechanical properties and failure behaviour of carbon fibre-reinforced polymer composites under the influence of moisture*. Composites A 1997;**28**:595–604.
4. Biro DA, Pleizer G, Deslandes Y. *Application of the microbond technique: effects of hydrothermal exposure on carbon-fiber/epoxy interfaces*. Comp Sci Tech 1993;**46**:293–301.
5. Zhou J, Lucas JP. *The effects of a water environment on anomalous absorption behavior in graphite/epoxy composites*. Comp Sci Tech 1995;**53**:57–64.
6. Ellyin F, *Master R. Environmental effects on the mechanical properties of glassfiber epoxy composite tubular specimens*. Comp Sci Tech 2004;**64**:1863–74.
7. Imaz JJ, Rodrigurz JL, Rubio A, Mondragon I. *Hydrothermal environment influence on water diffusion and mechanical behaviour of carbon fiber/epoxy laminates*. J Mater Sci Let 1991;**20**:662–5.
8. Wan YZ, Wang YL, Huang Y, He BM, Hah KY. *Hydrothermal aging behaviour of VARTMed three-dimensional braided carbon-epoxy composites under external stresses*. Composites A 2005;**36**:1102–9.
9. Shen CH, Springer GS. *Moisture absorption of graphite–epoxy composites immersed in liquids and in humid air*. J Comp Mater 1976;**10**:2–20.
10. Collings TA, Copley SM. *On the accelerated aging of CFRP*. Composites 1983;**14**:180–8.
11. Bullions TA, Loos AC, McGrath JE. *Moisture sorption effects and properties of a carbon fiber-reinforced phenylethynyl-terminated poly(etherimide)*. J Comp Mater 2003;**37**:791–809.
12. Liao K, Tan YM. *Influence of moisture-induced stress on in situ fiber strength degradation of unidirectional polymer composite*. Composites B 2001;**32**:365–70.
13. Luo HL, Lian JJ, Wan YZ, Huang Y, Wang YL, Jiang HJ. *Moisture absorption in VARTMed three dimensional braided carbon–epoxy composites with different interface conditions*. Mater Sci and Eng A 2006;**425**:70–7.
14. Thwe MM, Liao K. *Effects of environmental aging on the mechanical properties of bamboo–glass fiber reinforced polymer matrix hybrid composites*. Composites A 2002;**33**:43–52.
15. Wan YZ, Wang YL, Huang Y, Luo HL, He F, Chen GC. *Moisture absorption in three-dimensional braided carbon/Kevlar/epoxy hybrid composite for orthopedic usage and its influence on mechanical performance*. Composites A 2006;**37**:1480–4.

16. Lee MC, Peppas NA. *Water transport in graphite/epoxy composites*. J Appl Polym Sci 1993;**47**:1349–59.
17. Loos AC, Springer GS. *Moisture absorption of graphite-epoxy composites immersed in liquids and in humid air*. J Comp Mater 1979;**13**:131–47.
18. Alawar A, Bosze EJ, Nutt SR. *A hybrid numerical method for calculation of sag of composite conductors*. Electr Pow Syst Delivery 2006;**76**(5):389–94.
19. Crank J. *The mathematics of diffusion*, 2nd ed. p. 71–4.
20. Boyd J, Chang G, Webb W, Speak S. *Galvanic corrosion effects on carbon fiber composites*. In: 36th International SAMPE symposium and exhibition: how concept becomes reality, April 15–18, 1991; p. 1217–31.
21. Boyd J and Speak S. *Galvanic corrosion effects on carbon fiber composites: results from accelerated tests*. In: 37th International SAMPE symposium and exhibition: materials working for you in the 21st century, March 9–12, 1992; p. 1184–98.
22. Wang HT, Smith JM. *Tortuosity factor of diffusion in catalyst pellets*. ALChE J 1983;**29**:132–6.
23. Bourg IC, Sposito G, Bourg ACM. *The tortuosity of diffusion paths in saturated compacted sodium bentonite*. Clays in natural & engineered barriers for radioactive waste confinement 2005:149–50.